Journal of Quantitative Spectroscopy & Radiative Transfer 334 (2025) 109364

Contents lists available at ScienceDirect

Journal of Quantitative Spectroscopy and Radiative Transfer

journal homepage: www.elsevier.com/locate/jqsrt

Exploring the impact of rainfall intensity on the attenuation-rainfall relationship

Saeid Esmaeil Nia [a,b,*], Ali Shokri [a]

[a] School of Engineering, The University of Waikato, Hamilton, New Zealand
[b] Toi Ohomai Institute of Technology, 70 Windermere Drive, Poike, Tauranga 3112, New Zealand

ARTICLE INFO

Keywords:
Attenuation
Microwave
Cross-section
Rainfall intensity
Mie scattering

ABSTRACT

The attenuation of electromagnetic waves due to rainfall is a critical factor in radar and telecommunication systems, particularly in frequency bands above 10 GHz, which is increasingly utilised for data transfer. This study addresses the gaps in understanding how these attenuation effects vary across different rainfall intensities and Drop Size Distributions (DSD). By analytically investigating the irregularities in the cross-sections of raindrops within the 1 to 30 GHz frequency range, the study mentions significant peaks in attenuation at frequencies below 10 GHz, which are more pronounced as DSD changes with rainfall intensity. Using the extinction and efficiency cross-sections of raindrops in 1–30 GHz microwave transmission, the coefficients of rainfall-attenuation correlation were derived for each sector of rainfall intensity of 1–300 mm/hr. Building on these findings, we propose an enhanced rainfall-attenuation relationship, incorporating dynamic coefficients, varying with both factors, DSD and rainfall intensity. Unlike previous models that only suggest calibration of the attenuation-rainfall relationship with DSD, our results indicate that the coefficients should also dynamically adjust based on rainfall intensity. We further demonstrate how these varying coefficients differ from the ITU's recommendations, providing detailed graphical comparisons. This advancement allows for more accurate calculations of rainfall intensity, improving the precision of telecommunication and radar systems in diverse weather conditions.

1. Introduction

Radio waves have been used for telecommunication for more than a century [1]. However, the primary focus on atmospheric effects, particularly rainfall, on microwave propagation, is raised only after World War II [1–3]. Weather meteors such as raindrops, snow folks, and water vapour can diminish the power of electromagnetic (EM) waves [4]. Therefore, the intensity of precipitation directly impacts the attenuation of the EM waves and the stability of the connection.

While these guidelines help ensure minimal signal interruption [5] a simple power correlation between rainfall intensity and attenuation is often used to measure the attenuation of EM waves in a rain event [6,7] The equation is usually presented as [8]:

$$\gamma_R = kR^{\alpha} \tag{1}$$

where γ_R is the specific attenuation (dB/km), R is the rainfall rate (mm/hr), and k and α are constants that are determined as functions of frequency.

On the other hand, the reverse correlation can also be implemented to estimate the rainfall intensity using the attenuation from microwave links:

$$R = aA^{b} \tag{2}$$

Where A is attenuation and a and b are constants.

By the application of the rainfall-attenuation relationship, microwave links were used for rainfall intensity monitoring in the late 1990s and early 2000s, [9–12]. In addition, Commercial Microwave Links (CMLs) with frequencies above 18 GHz are used as rain gauges in Israel and the Netherlands [13–15].

These equations have undergone revision and adjustment in recent years across many countries, from the Netherlands and Israel to other European nations, as well as Australia and Brazil [16]. Adjustments range from identifying local correlations and classifying dry and wet periods to establishing the baseline of the microwave signal, correcting for wet antenna effects, and mapping rainfall [16].

Typically, a unique A-R correlation is applied to a given area of

* Corresponding author.
E-mail address: saeid.esmaeilnia@toiohomai.ac.nz (S. Esmaeil Nia).

https://doi.org/10.1016/j.jqsrt.2025.109364
Received 9 March 2024; Received in revised form 18 September 2024; Accepted 14 January 2025
Available online 15 January 2025

study, based on recommendations, previous research, or local calibration. However, there are concerns about the accuracy of such correlations, as they are influenced by various factors.

The Eq. (2) is structured based on the effects of all raindrops on the microwave signal. Therefore, the total attenuation of EM waves passing through a rainfall event is dependent on Drop Size Distributions (DSD) [17–20]. DSD describes the statistical characteristics of the size of raindrops [21,22] and determines the average number of each size of raindrops during the rainfall event. In practice, exponential, gamma or log-normal distributions are the most common forms of DSD [23]. DSD curves show that the number of larger drops increases in heavier rainfalls [24–28].

Wave attenuation is the result of interaction between the targets, raindrops here, and the radiation. This interaction depends on the size of the drops or DSD patterns and could be described with the concept of scattering cross-section (C) [29]. The absorbed wave also describes the absorption cross-sections.

Since each location has its own unique DSD, Eq. (1) and Eq. (2) need to be calibrated with local constants. Improved adoption has been observed by adjusting Eq. (2) based on local DSD data [30,31]. Some studies also show that using ITU recommendations [8] for a and b constants of the attenuation-rainfall relationship can produce significant errors when the local DSD data is not applied [32].

On the other hand, DSD changes with rainfall intensity that means the number of raindrops in each size varies by rainfall intensity. Therefore, the coefficients α and k In Eq. (1) and a and b in Eq. (2) are dependent on the variation of attenuation in different rainfall intensities. However, the calibration only applies to the general local DSD and they do not change when the rainfall intensity changes.

The power-law relationship used for converting signal attenuation to rainfall does not account for variations in DSD and temperature, which can lead to significant errors in measurement [33]. Errors in microwave link rainfall estimates are influenced by spatial variations in DSD, indicating that a one-size-fits-all approach using constant coefficients may not be appropriate [30]. Another study also shows that uncertainties in rainfall maps derived from microwave links stem from various factors, including the sampling intervals and the inherent variability in rainfall characteristics [34].

In a rainfall radar study, underestimated peak rainfall intensity from 44 % to 67 % is discussed as a result of a fixed Z-R relationship, which does not account for natural variations in raindrop size distribution with varying rainfall intensity [35]. The radar reflectivity factor (Z) is the sum of the sixth power of each hydrometeor's diameter, calculated for all hydrometeors within a unit volume [36]. The radar reflectivity factor is a feature of the recipient objects and depends on DSD [37]. Therefore, weather radars use a similar relationship to the rainfall-attenuation, between the reflectivity of the microwave signal and rainfall intensity which inherently depends on rainfall intensity.

In this study, we aimed to address this gap by showing the effects of considering a varying rainfall rate in the rainfall-attenuation relationship. Finding those effects requires calculating attenuation for different rainfall rates and finding the best correlation in each range of rainfall intensity. A dataset which provides a precise number of droplets needs a rainfall measurement with disdrometers. Some studies have recorded rainfall intensity and attenuation of a microwave link in a setup in the Netherlands [38–40] and Australia [41] However, finding specific coefficients for different rainfall intensities in A-R relationship needs a classification of rainfall rates and the corresponding attenuation rate. This relationship is usually affected by other factors, like wind, temperature, and humidity which are not under control. Therefore, this research focused on an analytical study of attenuation and rainfall intensity and establishing the correlation between them.

In this study, analytical analysis of rainfall is established by finding the total number of each size of raindrops at a time. Attenuation is a result of extinction efficiency on all the raindrops in the electrical field of the microwave signal. Therefore, the study includes the calculation of extinction and efficiency cross-sections for a range of raindrop sizes across the 1 to 30 GHz frequency range. Then, the results are used to establish a relationship between attenuation and rainfall intensity, ranging 1 to 300 mm/hr, and find the correlation coefficients. The study particularly focuses on frequencies below 10 GHz, where previous literature has been limited.

The reason for paying attention to this range of frequencies is the importance of them in telecommunication area. More microwave links are available in lower frequencies. However, the attenuation in the frequencies from 1 to 3 GHz, which are commonly used between cell phones and Base Transceiver Station (BTS), is reported to be too low for rainfall monitoring [42–44]. There are also recommendations by some studies to use particular frequencies, such as above 5 GHz [45], 6 GHz [8], and 10 GHz [46], which are more suitable for measuring rainfall intensity and volume.

A few studies showed a detectable range for attenuation in lower frequencies to be used in attenuation-rainfall rate relationships [47]. However, the microwave link is recommended to be longer than 15 km and the quantisation step finer than 0.02 dB [48]. It is also reported that a decrease in frequency to lower than 10 GHz increases the average error of estimating rainfall [19]. In addition, some more recent studies suggest that the frequencies above 30 GHz correlate better with ground rainfall monitoring than the lower frequencies [49,50].

Therefore, suggesting a more precise correlation for A-R for lower frequencies can help to apply the method for a higher number of microwave links. Looking for more precise coefficients and correlations, this study tried to analyse the variation of scattering cross-sections to detect the variation of attenuation of microwaves particularly below 10 GHz frequency and in different rainfall intensities. Considering the selected range is the most commonly used frequency band in cell phone telecommunication networks, including 3 G, 4 G, and 5 G generations [51,52] this paper explores the unfulfilled potential and limitation of using a lower frequency range from 1 to 10 GHz for rainfall monitoring.

2. Methods and results

2.1. Scattering approximations

James Clerk Maxwell was the first to formulate EM waves' fundamentals in the 19th century [53]. Later, Waterman [54] solved Maxwell's equations for scattering light by non-spherical particles and introduced the "T-matrix" approach [55]. Scattering theories, such as Mie and Rayleigh scattering, were developed to solve these equations for waves interacting with particles within a space [56–58]. These theories allow for calculating the impact of particles on microwave signals using scattering cross-sections.

Rayleigh scattering region applies when the particle with the radius r and refractive index n is electrically small ($2\pi r/\lambda \ll 1$) [59]. Mie scattering is applicable for particles with a reasonably big enough size to be independent of the wavelength [60], with a diameter equal to or larger than the wavelength. The scattering cross-section thus more depends on the relative size of the particle to the wavelength and angle of radiation meaning it is linked to the particle's volume [61].

Raindrop size is constrained by air resistance, with drops larger than 6 mm becoming unstable and splitting due to drag forces [62–66]. Smaller drops in the range of 0.2 to 0.5 mm in diameter are assumed to drizzle [67]. Additionally, the shape of raindrops evolves as they grow, transitioning from spherical to more flattened forms [59,68,69]. These size and shape characteristics influence scattering behaviour and, consequently, the overall attenuation of microwaves in rainfall.

Raindrops scatter a portion of the power of the irradiance into all directions. While defining the exact size and shape of raindrops improves the approximation of the attenuation, the scattering cross-section for a wavelength of λ and particle size of r is [70]:

$$C_{sca}(\lambda, r) = \frac{W_{sca}}{I} \tag{3}$$

where C_{sca} is the scattering cross-section (m^2), W_{sca} is the amount of power that is scattered (W), and I is the irradiance (Wm^{-2}). The scattering efficiency (Q_{sca}), is the ratio of the scattering cross-section to the geometric cross-section [70]:

$$Q_{sca}(\lambda, r) = \frac{C_{sca}}{A} \tag{4}$$

where, Q_{sca} the scattering efficiency (dimensionless), and A is the geometrical cross-section (m^2). The energy scattered ($\widetilde{F}_{sca}$) or absorbed by a particle ($\widetilde{F}_{abs}$) is proportional to the incident energy [71]:

$$\widetilde{F}_{sca} = C_{sca}F_0 \tag{5}$$

$$\widetilde{F}_{abs} = C_{abs}F_0 \tag{6}$$

where F_0 is the incident intensity of the radiation, $\widetilde{F}_{sca}$ and $\widetilde{F}_{abs}$ are scattered and absorbed intensities, and C_{abs} is the absorption cross-section. Therefore, the particle size and its proportion to the wavelength are the main ruling criteria in scattering theories.

Finally the total attenuation can be calculated from the extinction efficiency as [72]:

$$A = 4.343 \int_0^{\infty} N(D) Q_{ext}(D, \lambda, m) dD \tag{7}$$

where N is the number density of drops with diameter D or concentration of droplets within a given volume, Q_{ext} is the extinction efficiency which depends on, diameter (D), frequency (λ), and the complex refraction coefficient of raindrops (m) and dD is the drop diameter interval.

Therefore, in a rainfall event, a combination of DSD and the scattering/absorption cross-section of water drops in the air is implemented to predict rainfall attenuation [73,74]. The total attenuation between two antennas summarises all drops' effects on the wave by their corresponding cross-section [19,20].

For this study, two software packages, MiePlot [75] and COMSOL [76] were used to calculate the scattering and absorption cross-sections of raindrops across various microwave frequencies. These calculations allow for the analysis of how individual droplet sizes affect specific wave frequencies and assess the cumulative impact of all droplets.

For simplification, raindrops are assumed to be spherical in this study. This assumption enables direct comparison with previous studies, as Mishchenko [55] demonstrated that the T-matrix method reduces to Mie scattering theory for spherical particles.

Droplet diameters ranging from 1 mm to 10 mm were selected for Mie scattering calculations. The upper limit exceeds typical raindrop sizes to provide insights into the behavior of scattering cross-sections at lower frequencies. Droplets smaller than 1 mm were excluded due to their negligible contribution to the cross-sections, optimising computational time and efficiency.

Extinction cross-section and efficiency were calculated for the frequencies between 1 and 30 GHz. This is the microwave range where precipitation and gas absorption can cause problems especially at the higher end and over longer distances [77]. This frequency band is crucial for telecommunications [78,79].

Regarding the application of EM waves in telecommunication, previous studies have calculated cross-sections for droplets in frequencies above 10 GHz. For example, studies have been carried out for a range of 10 to 100 GHz [80], or some specific frequencies like 10, 30, and 120 GHz in one study [43] and 30, 60, and 120 GHz in another study [42]. A single 34.8 GHz frequency [81] is also getting more attention due to a higher application for communication purposes. However, the frequencies, which are lower than the recommendations for rainfall measurements [8] [45,46], are largely ignored in the literature in this regard. Limited studies focused on frequency ranges as low as 0.6 GHz [82] and 1 GHz [83]. However, they focused on specific frequencies, not the entire range. As a result, the lower frequency spectrum remains less explored for rainfall attenuation.

Looking for a detailed study of cross-sections in microwave range, Mie scattering was utilised through MiePlot software to calculate extinction efficiency (Q_{ext}) to detect the effects of individual drops confronting waves. Fig. 1 shows changes in extinction efficiency (Q_{ext}) in this range of diameter against different frequencies.

In frequencies 1 to 3 GHz, Q_{ext} remains relatively low, indicating minimal impact on the wave by raindrop-sized droplets. However, in frequencies above 4 GHz, Q_{ext} increases gradually by increasing the frequency. Also, a contradiction could be observed in the form of a particular peak that appears at 4 GHz in around 8 mm drops and slide towards 3.5 mm diameter drops at 10 GHz. The peak flattens in 20 GHz and 30 GHz.

2.2. The effects of the complex refractive index

The refractive index is related to the change of velocity of electromagnetic waves in a medium regarding a vacuum [84]. The refractive indices of meteors are composed of a real and an imaginary part. The real part of the refractive index refers to the scattering wave, while the imaginary part is related to the absorption by the material [84–86]. The refractive index also varies by changing frequency [87].

At the next step, the wave propagation is simulated with only the real part of the refractive index to see what happens when the microwave hits the drop. This simulation, therefore, distinguishes some special effects of wave number on scattering patterns inside and around a droplet. As a result, when the ratio of wavelength to the drop diameter varies, some unique patterns of wave propagation appear in the electric field of the mediums of air and the particle.

In these simulations, the absorption part in wave propagation is set aside by assuming the imaginary part of the refractive index in MiePlot equal to zero. Then, calculations are applied for the same frequencies in Fig. 1 for calculating C_{ext}. The results are presented in Fig. 2 with the (R) curve for only the real part of the refractive index and the (R&I) curve for calculations using a refractive index including the real and the imaginary parts together.

In comparison with Q_{ext} curves and considering Eq. (4), peaks disappear at 8 GHz and above. Fig. 2 illustrates that the smooth peaks in frequencies of 4 to 8 GHz in the (R&I) curve turn to sharp peaks in the (R) curve, which is scattering without absorption. For example, at 5 GHz and (R&I) line, a drop diameter of 7.18 mm shows a peak C_{ext} of 65.1 mm^2. In the (R) graph, this smooth peak appears in a sharp peak of 1680 mm^2 in a 6.89 mm diameter drop.

The value of C_{ext} peaks decrease in higher frequencies at the R graph. The high rates fall to 839 mm^2 at 7 GHz and 505 mm^2 at 10 GHz. The peaks at 20 and 30 GHz are around 200 to 400 mm^2. However, they appear more frequently in more drops in the range of raindrops diameter.

While the imaginary part of the refractive index is omitted in simulating waves, the sharp peaks in scattering cross-sections generate some unique situations in wave scattering, refraction, and reflection. At the next stage, visualising the simulation of wave equations can display the patterns of electric field and hence the wave propagation inside and around the drops.

2.3. Numerical solution of Maxwell equations

For comparison, the Maxwell equations are solved to show the scattering patterns of electromagnetic waves confronting raindrops by focusing and emphasising their sizes. The solution was achieved using COMSOL Multiphysics, a comprehensive simulation software

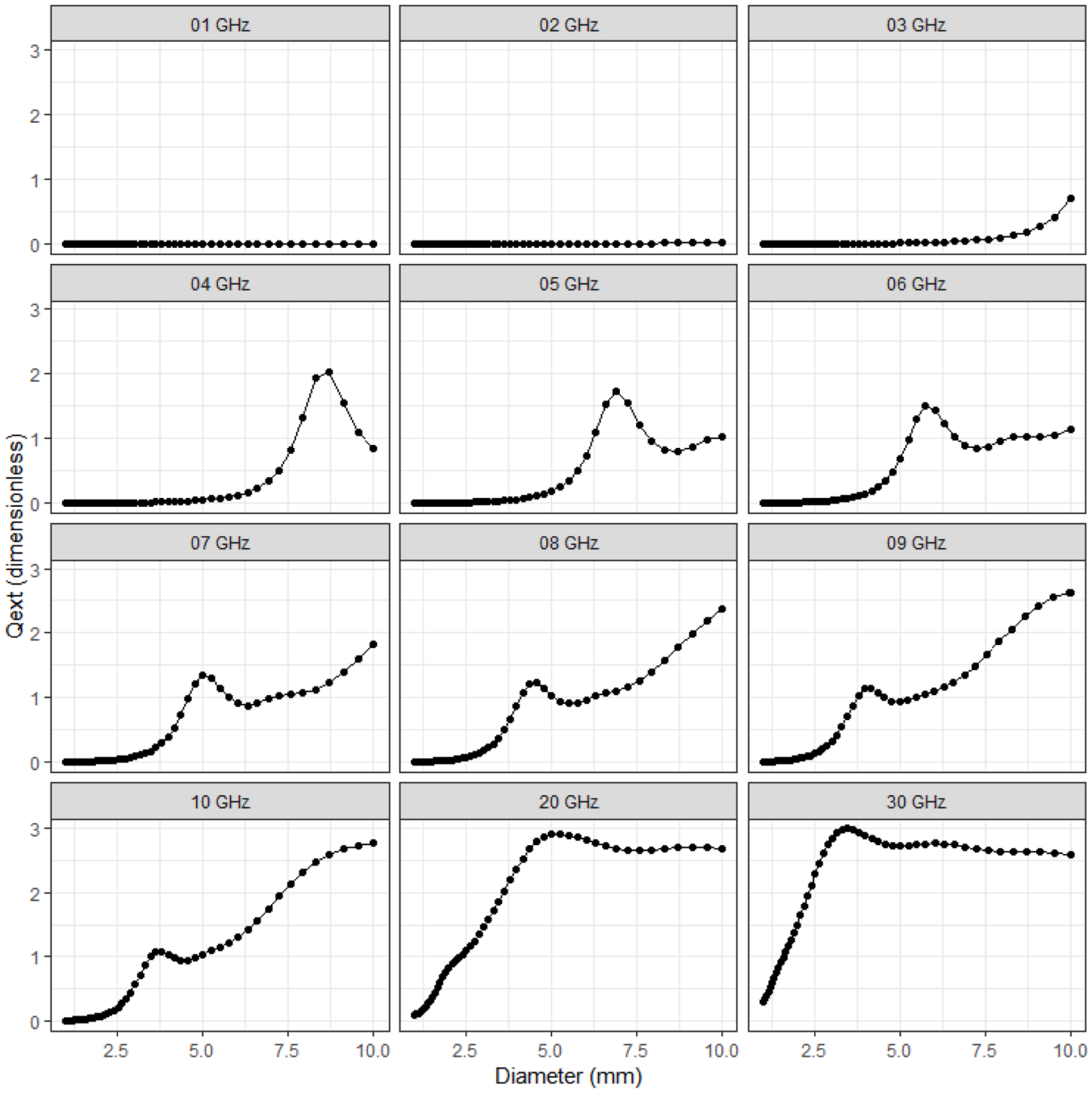

Fig. 1. Extinction efficiency of different diameters of water drops in frequencies 1 to 10 GHz, 20 GHz, and 30 GHz using MiePlot.

environment for a wide range of applications [76]. COMSOL simulations can illustrate the wave pattern inside and around a drop. Unlike the scattering-approximations approach, solving the Maxwell equations calculate electric and magnetic fields for space points in time steps and describes the spreading of the electromagnetic wave [88]. Therefore, the electromagnetic field change inside and around the droplets could be observed instead of a black-box simulation.

2.4. Cross-section calculations in COMSOL

Simulations of drops and electromagnetic waves are carried out using the radio frequency module and the frequency domain. In the first step, the imaginary part of the complex refractive index is set to zero for the electric field displacement model to solve the wave equation. Then, the three-dimensional simulation is set up with a water drop in a spherical space surrounded by a perfectly matched layer [89,90] Fig. 3 shows the simulation setup and mesh in COMSOL. The drop and surroundings and technical details followed the method used by Garcia-Etxarri [89].

In this model, the mathematical relations calculate scattering and absorption cross-sections through the power of the wave and the diameter of the drops. The absorption cross-section (C_{abs}) indicates the amount of the absorbed incident wave and is defined as:

$$C_{abs} = \frac{1}{I_0}\int_v d^3xQ \tag{8}$$

where the integral is calculated over the droplet volume and Q is the

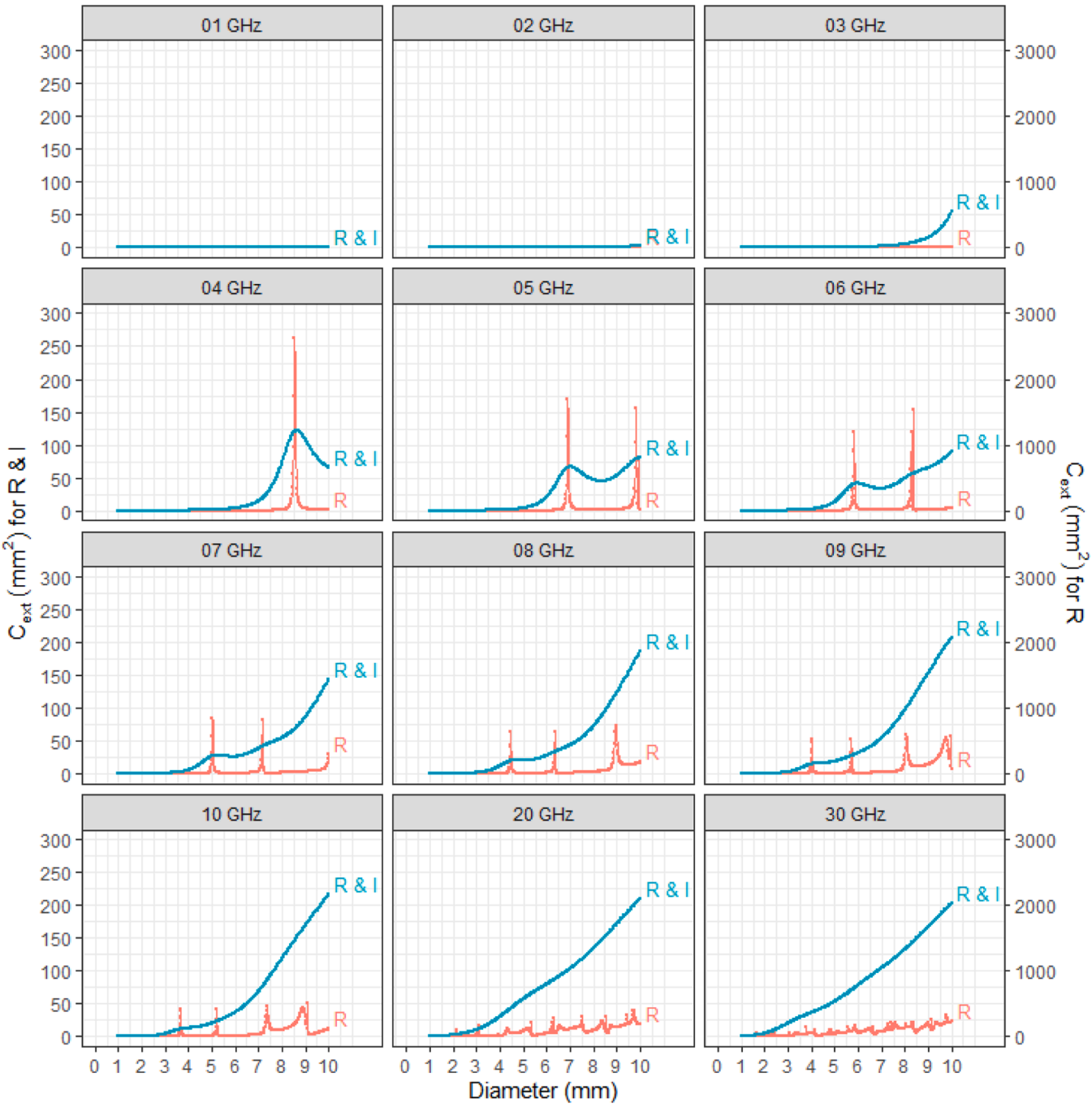

Fig. 2. Extinction cross-sections calculated, (R&I): with the real and the imaginary part of the refractive index, (R): with the real part and zero imaginary part (using MiePlot).

power loss density in the particle. d is drop diameter and I_0 is the incident energy. The scattering cross-section (C_{sca}) describes the amount of the wave, scattered away on the droplet and is defined as:

$$C_{sca} = \frac{1}{I_0} \int_s d^2x \bar{n} \cdot \overline{S_{sca}} \tag{9}$$

where $\bar{n}$ is the normal vector pointing outwards normal to the droplet and $\overline{S_{sca}}$ is the pointing vector. The extinction cross-section determines the lost wave and is given by the sum of the absorption and scattering cross-section:

$$C_{ext} = C_{abs} + C_{sca} \tag{10}$$

The COMSOL simulation results cross-section in the same range as MiePlot, either with or without the imaginary part of the refractive index. Further steps in analysing the propagation of microwaves among droplets could simulate the dynamic behaviour of microwaves confronting a droplet. The setup in COMSOL with a time-dependant radiofrequency module is used to display how the drop size affects the wave when the wave enters and exits a droplet.

2.5. Illustration of scattering waves in COMSOL

Simulating the electric field surrounding a raindrop can show how various diameters of a raindrop impact wave propagation differently. Therefore, raindrop diameters are altered from 1 mm to 10 mm in

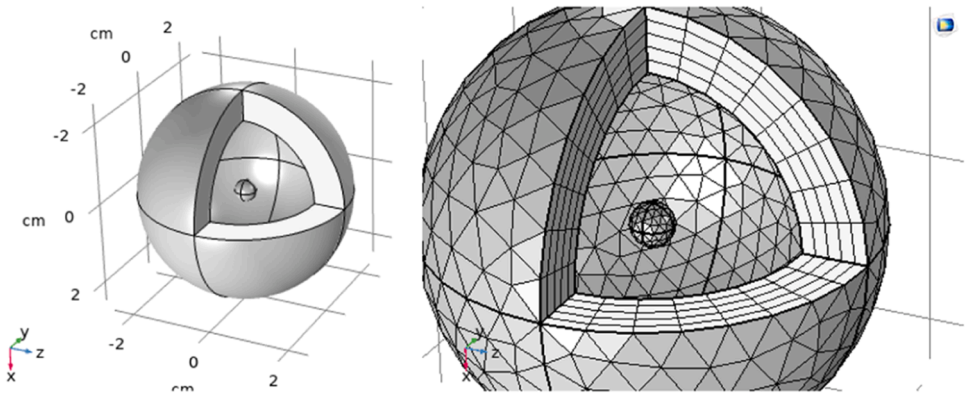

Fig. 3. Left: The sphere inside as a water drop and the sphere around for perfectly matched layer in COMSOL, Right: Simulation mesh for two spheres

increments of 0.1 mm to simulate the electric field surrounding a raindrop and estimate the scattering cross-section curves previously shown in Fig. 2.

The electric field simulated in COMSOL Shows the same trends, similar to the curves of cross-sections calculated by MiePlot. The electric field inside the drops shows an increase in particular diameters which shows a peak in the extinction cross-section.

Fig. 4 shows the 3D simulations of the electric field in a 2D section with no imaginary part of the refractive index. For each frequency, the drops which show a peak in cross-section, compared to a few smaller and larger drops. For example, in the first row, in the frequency of 5 GHz, the maximum electric field occurs in a droplet with a 6.9 mm diameter, similar to MiePlot in Fig. 2. Likewise, at 7 GHz, the maximum electric field occurs in droplets with around 5.0 mm and 7.2 mm diameters, which validates the MiePlot findings.

Also, a Fast Fourier Transform (FFT) is added to the frequency domain to observe the electric field variation. The simulation in a picosecond time frame is carried out for a 5 mm droplet to focus on electric field changes when the droplet confronts a 7 GHz electromagnetic wave and the results as an electric field are shown in Fig. 5. Each timestep shows how the wave penetrates the droplet and how different amounts of reflection and refraction occur on the inner and outer walls of the droplet.

The dark red colour inside the drop, in time steps 45 and 50 ps, demonstrates the concentrated electric field in the droplet due to the repetitive reflection of the wave on the inner walls of the droplet before exiting the droplet.

2.6. *Analysing the impact of cross-section variations on rainfall calculation*

The cross-section variations indicate that microwave signals at

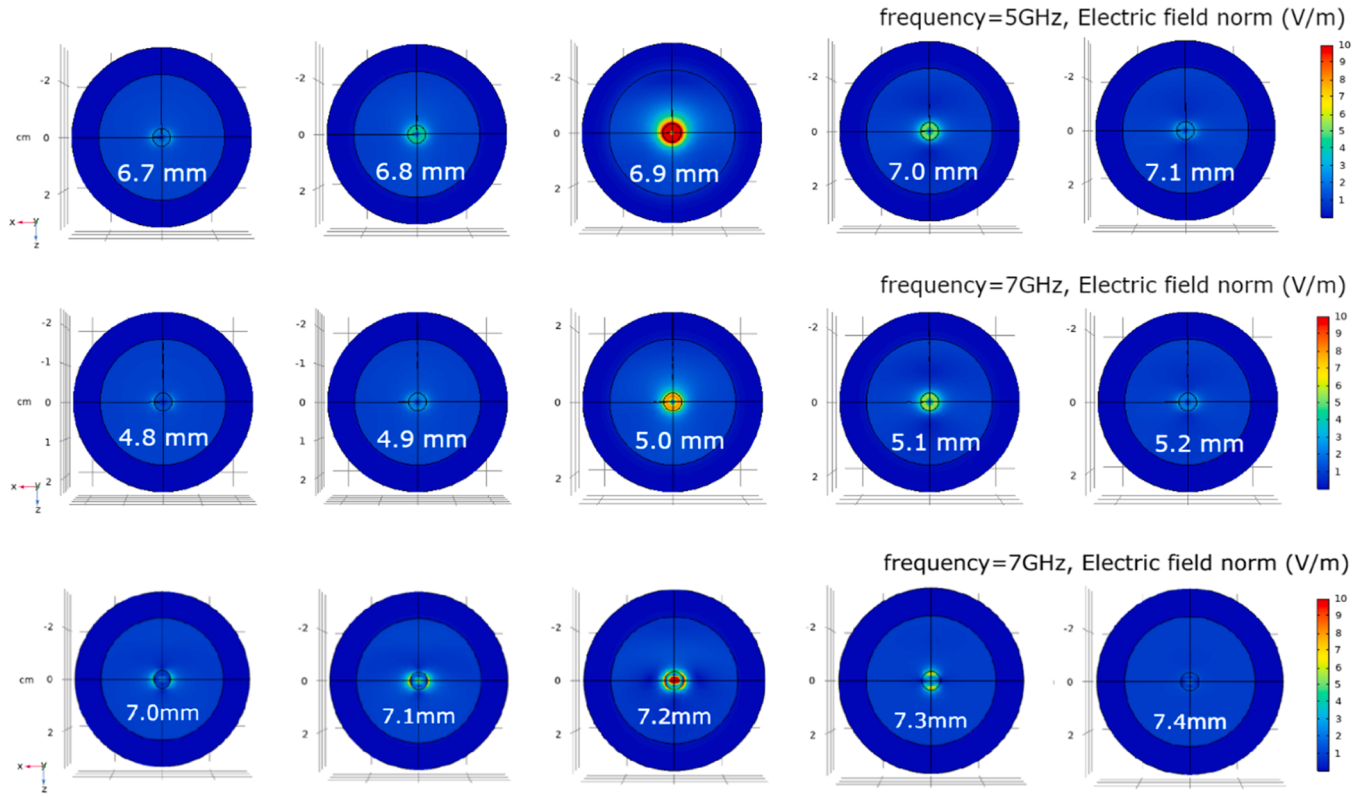

Fig. 4. The electric field simulation inside and around the drops, from top to bottom, one peak in 5 GHz frequency, appears in 6.9 mm diameter, and two peaks in 7 GHz frequency appear in 5.0 mm and 7.2 mm diameters.

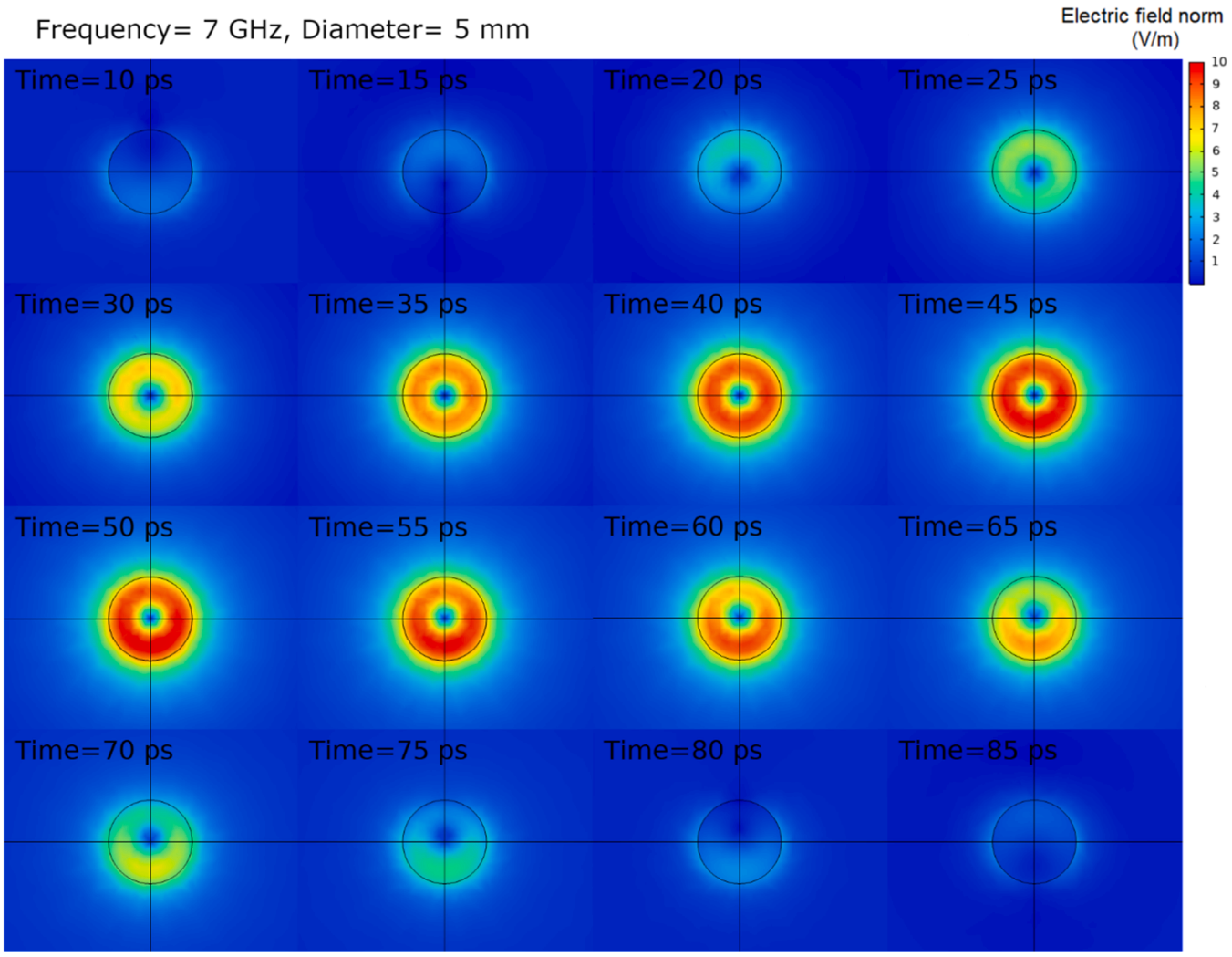

Fig. 5. Electric field inside and around a 5 mm diameter droplet in time steps 10 to 85 picoseconds with a 7 GHz wave. (Imaginary part of refractive index = 0).

various frequencies exhibit distinct behaviours when traversing through raindrops. This discrepancy arises from the varied responses of each raindrop size to the signal mixing with the different raindrop size distribution in different rainfall intensities. Consequently, regarding the cross-section analysis and extinction calculations across different frequencies, it is anticipated observing diverse correlations between attenuation and rainfall.

According to various hypothetical drop size distributions (DSD) it is possible to analyse the total attenuation resulting from any rainfall intensity. The combination of DSD from rainfall intensity and cross-section values for each frequency and drop size, results in the total attenuation for the rainfall intensity.

The amount of rainfall is the sum of all drops falls on a surface at one moment:

$$R = \sum_{D_{min}}^{D_{max}} \nu(D_i) N(D_i) V(D_i) \tag{11}$$

where R is rainfall rate, D is the diameter of the raindrop, $\nu(D_i)$ is raindrop velocity, $N(D_i)$ is drops size distribution (or number of each size of drops), and $\nu(D_i)$ is the volume of the raindrop.

Now, combining Eq. (11) with Eq. (7) and applying them to Eq. (1) results in different coefficients of the power law for each frequency. The different coefficients of Eq. (1) are calculated by International Telecommunication Union recommendations P-838.3 [8]. The constants are suggested for horizontal and vertical polarised signals. The constants are k_H and α_H for Horizontal polarisation and k_V and α_V for vertical polarisation.

Fig. 6 and Fig. 7 show the k and α variations in Eq. (1) for frequency

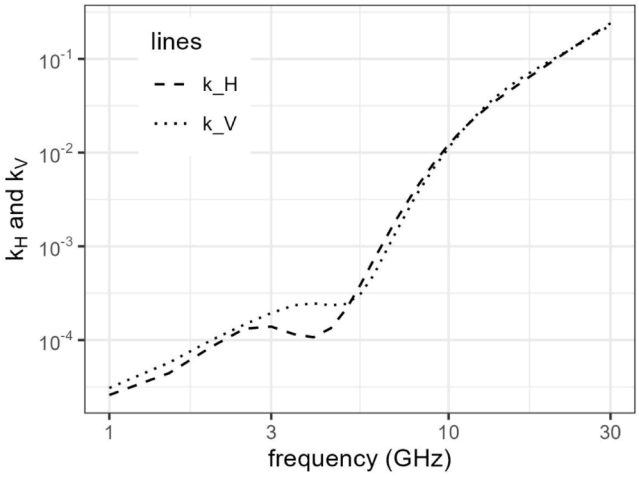

Fig. 6. k coefficient in Eq. (1) for horizontal and vertical polarisations. (regenerated from [8]).

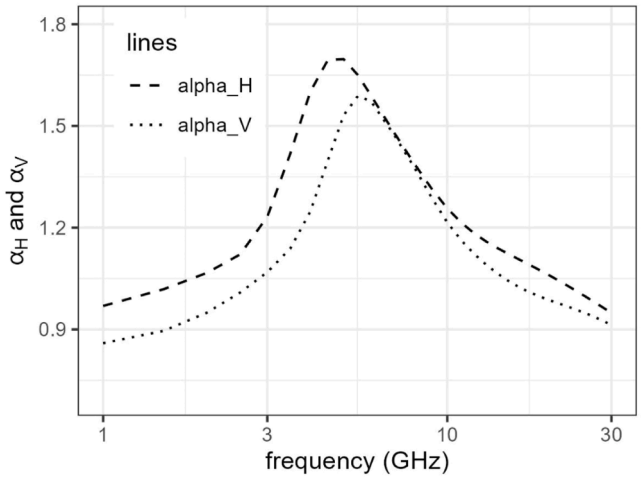

Fig. 7. Alpha coefficient in Eq. (1) for horizontal and vertical polarisations. (regenerated from [8]).

range of 1 to 30 GHz, generated from ITU-R P-838.3 [8].

Combination of Eq. (7), Eq. (11), and Eq. (2) results:

$$R = a\left(4.343\int_0^{\infty} N(D)Q_t(D,\lambda,m)dD\right)^b \tag{12}$$

Various rainfall intensities yield different $N(D)$ values which cause different attenuation rates. Knowing rainfall and attenuation, the constants a and b can be derived and calibrated for real conditions. It is important to note that these coefficients are dependent upon the intensity of rainfall.

Analysis needs to define a model for drop size distribution. There are different drop size distribution models suggested to calculate $N(D)$. Marshall and Palmer distribution is one of the first DSD models widely used and investigated in rainfall research, derived through the fitting of empirical data obtained in Ottawa, Canada, in 1946 [65]. Better distributions are suggested for the raindrop size distribution based on Gamma distribution [73] and Weibull distribution, like Sekine-Lind model [91].

The Marshall-Palmer model also known for its simplicity and structure, is better for representing raindrop size distribution in light to moderate rainfall. In contrast, the Sekine-Lind model, with its multiple parameters, offers a more detailed and flexible representation of DSD, capable of capturing complex rainfall characteristics across various conditions.

Gamma DSD models are more commonly used compared to the Weibull model, but they have fewer parameters and are likely less sensitive to variations in rainfall intensity. While Weibull and Log-Normal distributions can capture the lower number of small drops, Gamma and exponential distributions are less effective in modelling the variation in this range. Notably, the Weibull model can resemble the Gamma model when the appropriate coefficients are selected.

Therefore, in this study, the Marshall-Palmer and Sekine-Lind models were chosen to represent the minimum and maximum influence of rainfall intensity variation, which aligns with the study's objective to detect these effects.

For calculating attenuation and the Rainfall-Attenuation relationship, droplets ranging from 0.2 mm to 11 mm with 0.2 mm intervals were modelled in COMSOL. These intervals were chosen to minimize simulation time, given the limitations of available computational resources. To ensure accuracy and check for any irregularities or potential peaks that might not be captured by COMSOL, we also generated output in MiePlot for droplets ranging from 0.2 mm to 12 mm with increments from 0.0025 to 0.03 mm. MiePlot results showed no unexpected peaks beyond those observed in COMSOL. The size range used in COMSOL aligns with the actual range of raindrop sizes in DSD models, allowing us to generate rainfall intensities between 1 and 300 mm/hr.

DSD models generate some values for $N(D)$. A sequence of $N(D)$ values is calculated to investigate the influence of variations in rainfall intensity. To find the coefficients, Eq. (11) is used to relate rainfall intensity to DSD. Then, Eq. (7) is used to produce attenuation for that rainfall intensity. In the next step, a series of attenuation-rainfall values in the range of ±10mm/hr selected to stablish the A-R correlation to ascertain the constants a and b.

Fig. 8 displays the outcomes of b calculations derived from the rainfall-attenuation correlation (Eq. (2)), resolved for various rainfall intensities using a Marshall-Palmer drop size distribution (DSD). Fig. 9 is the same calculations using a Sekine-Lind distribution. The dotted and dashed lines in these graphs represent ITU P-838.3 recommendations [8] for horizontal and vertical polarisations respectively. b_H and b_V are calculated by substituting α_H and α_V from Eq. (1) and Eq. (2). Ten blue lines depict the variations in b for rainfall intensities between 1 and 300 mm/hr in steps of 20 mm/hr solved for each DSD model with spherical raindrops. Therefore, the 100 mm/hr curve is related to calculating DSD for rainfall intensities between 90 and 110 mm/hr while the 200 mm/hr curve is for calculating DSD from 190 to 210 mm/hr.

Rainfall intensities above 300 mm/hr are considered extremely rare and are typically regarded as unrealistic in hydrological studies.

As depicted in results, the drop size distribution significantly impacts the b values. In Fig. 8, b values fall within the ITU recommendation range for rainfall intensities between 20 and 30 mm/hr at frequencies higher than 10 GHz and rainfall intensities between 30 and 300 mm/hr in frequencies <4 GHz. However, b values surpass the ITU recommendations at frequencies higher than 10 GHz and rainfall intensities higher than 30 mm/hr.

In Fig. 9 with Sekine-Lind model, the b values are consistently lower than the ITU recommendations in frequencies <25 GHz. A significant change is decreasing b with increasing rainfall intensity in frequencies lower than 5 GHz which changes to an increasing b in higher frequencies. rainfall

The least variation in b occurs in the frequencies 15 and 1 GHz. In both distributions, b generally decreases with increasing rainfall intensities at frequencies below 5 GHz, while at higher frequencies, b increases with rising rainfall intensities.

The other coefficients are α_H and α_V in Eq. (1) which is correlated with a_H and a_V in Eq. (2) which are simply the reverse of each other. Fig. 10 and Fig. 11 present the coefficients α_H and α_V in Eq. (1) as recommended by ITU [8] and as calculated for different rainfall intensities from Eq. (1), Eq. (7), and Eq. (11) for different DSD models.

Fig. 10 uses the Marshall-Palmer model for DSD. The variation of α for spherical drops is limited to 0.4. α increases by increasing rainfall

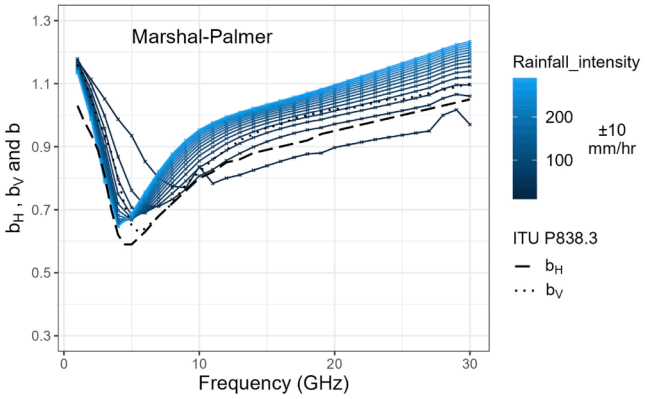

Fig. 8. b_H and b_V derived from ITU P-838.3 recommendation and b for attenuation-rainfall power law with spherical rain drops and Marshall-Palmer drop size distribution.

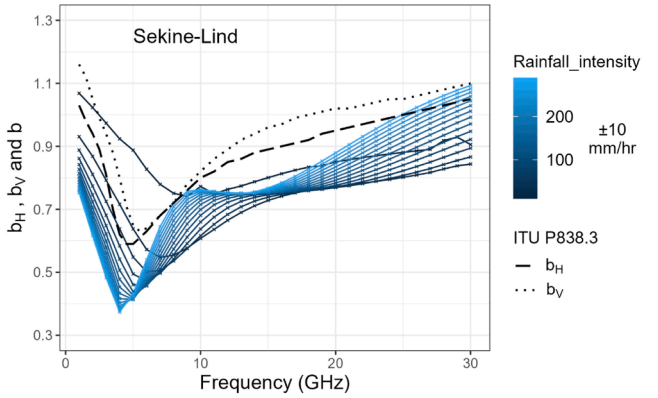

Fig. 9. b_H and b_V for ITU P-838.3 recommendation and b for attenuation-rainfall power law with spherical rai drops and Sekine-Lind drop size distribution.

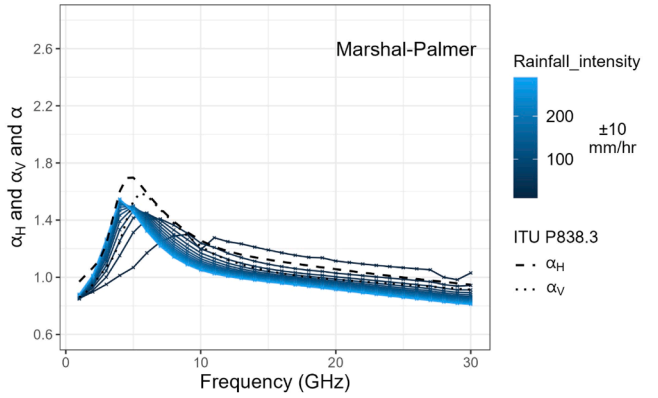

Fig. 10. The coefficient α in power law for different rainfall intensities and frequencies with a Marshall-Palmer DSD model.

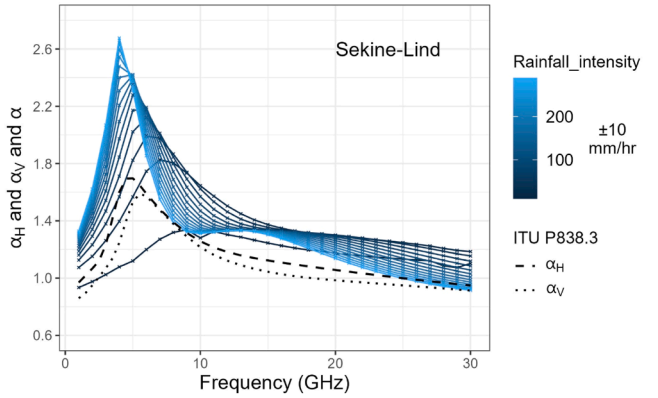

Fig. 11. The coefficient α in power law for different rainfall intensities and frequencies with a Sekine-Lind DSD model.

intensity at frequencies <5 GHz while decreasing at higher frequencies.

In Fig. 11 the same calculations are conducted using the Sekine-Lind model. The variation in α is greater here. Like the Marshall-Palmer model, the variation trends are different below and above 5 GHz. However, the range of changes in the Sekine-Lind model is considerably greater and does not accord with the ITU recommendations.

2.7. Suggesting adjustment in formulas

Considering the variation of DSD and consequently $N(D)$ with rainfall intensities, and as Fig. 8–Fig. 11 illustrate, Eq. (12) is proposed to be adjusted, considering a and b changing with rainfall intensity:

$$R = 4.343 \cdot a_i \left(\int_0^\infty N_i(D) Q_{ti}(D, \lambda, m) dD \right)^{b_i} \tag{13}$$

Where a_i and b_i are supposed to be different for each rainfall intensity.

This equation can be transformed into the well-known rainfall-attenuation formula with varying coefficients to be used in rainfall measurement:

$$R = a_i A^{b_i} \tag{14}$$

This equation introduces variable coefficients for calculating rainfall from attenuation, with a_i and b_i dependent on rainfall intensity. As a result, the calculation involves an iterative loop. Starting with an assumed rainfall intensity, corresponding values for a_i and b_i are determined, which then yield a new rainfall estimate. This updated rainfall rate generates a new set of a_i and b_i values, leading to another recalculated rainfall rate. The process continues, with each iteration producing a new rainfall estimate, until the change between successive rainfall rates becomes minimal, signalling convergence.

3. Discussion

The distribution of raindrop sizes, represented by $N(D)$ or DSD, plays a crucial role in determining the overall attenuation, with certain drops exerting a greater influence on cross-section. The collective impact of these influential drops, determined by the total number of occurrences, can substantially contribute to the overall attenuation. Simulating with zero refractive index underscored the C_{ext} variation among different drop sizes.

The results of analytical correlation between attenuation and rainfall using different DSD models show that the coefficients of the rainfall-attenuation power law are not constant. They change in different rainfall intensities. Therefore, it is needed to use different coefficients for a lower or higher rainfall intensity to achieve a better rainfall-attenuation correlation.

Calculations on such a varying coefficient is not straightforward. At first, the constants a and b vary with frequency as ITU recommends and the results prove. On the other hand, given that $N(D_i)$ relies on rainfall intensity and both a and b are contingent on rainfall intensity, the parameters are interconnected in a circular manner. Rainfall is calculated from attenuation influenced by a and b, and these coefficients, in turn, hinge on rainfall intensity. However, it is noteworthy that rainfall intensity itself remains undefined and necessitates the definition of a and b. Consequently, employing specific methods such as iteration may prove instrumental in solving the equation.

The results of the study illustrate and emphasise the behaviour differences between the extinction cross-sections of droplets in frequencies less and >10 GHz. Simulation of electric field and calculating extinction cross-sections of drops using Mie scattering theory and Maxwell equations showed similar results in illustrating the behaviour of microwave signals in different frequencies.

The value of cross-sections alone is not able to describe the attenuation-rainfall relationship. The total attenuation is a result of multiplying cross-sections by the number of raindrops in rainfall events which is represented as DSD.

The effect of DSD on the attenuation-rainfall relationship is that when rainfall intensity increases, larger drops appear, and the total attenuation increases. This is in addition to an increase in the total number of raindrops. Meanwhile, in higher frequencies, the cross-sections increase gradually, and the appearance of larger drops affects the total attenuation gradually and ascendingly. However, for lower

frequencies, the total attenuation may decrease when a high rainfall intensity contains droplets with a larger size than the cross-section peak range. Decreasing attenuation, while the rainfall intensity is increasing, results in a lower rate of increase for attenuation in comparison with the rainfall. Then, the attenuation-rainfall trendline needs to be corrected after reaching a particular rainfall intensity. This variation in total attenuation can describe the different behaviour of the coefficients at frequencies lower and higher than 5 GHz.

As depicted in the graphs, the coefficients of the power law exhibit greater uniformity and stability when employing the Marshall-Palmer model, in contrast to the Sekine-Lind model. This disparity underscores the significance of the Drop Size Distribution (DSD) model in rainfall calculations. Consequently, it is imperative to thoroughly investigate and define the appropriate DSD model, calibrating the equations to local conditions.

Cross-section calculations determined some features of the droplets, Results show some significant impact on some particular drop sizes in lower frequencies affects the total attenuation. Findings of the study showed some distinctive peaks in extinction cross-sections in frequencies lower than 10 GHz. Peaks were amplified by simulating with a zero imaginary part of the refractive index. The peaks appeared in the range of the diameter of raindrops in frequencies 6–9 GHz. These peaks were not presented in higher frequencies (20 and 30 GHz), or they are flatter.

Simulating microwaves with different refractive indices may illustrate some unique patterns of reflexing waves inside a droplet and magnify their impact. Considering a complex refractive index with or without the imaginary part assisted the simulations in pointing out those sizes of drops. The real part of the complex refractive index refers to the scattering wave, while the imaginary part is related to the absorption by the material [85,86].

Therefore, utilising both the real and the imaginary parts produces total power loss. However, ignoring the imaginary part produces patterns of scattering waves inside and around the particle, which can distinguish the reflection of the wave inside some particular diameters of droplets. Therefore, the real part of the refractive index shows how repetitive reflecting happens inside a droplet before the wave exits the drop. In this condition, the path of the wavefront can be followed.

Measuring rainfall using microwave links at frequencies below 10 GHz is theoretically feasible if the attenuation can be accurately measured. However, a significant challenge arises due to the lower total power attenuation in these lower frequencies, which may not always be detectable. The lower values of scattering cross-sections in frequencies of 1 to 4 GHz could be a real obstacle to using these frequencies in rainfall measurement. In comparison, although scattering cross-sections in frequencies of 4 to 10 GHz are still relatively lower than 20–30 GHz, the appearance of some peak values in the larger drops can significantly increase the attenuation in heavy rainfall events. Therefore, long microwave links covering more raindrops can show some measurable attenuation values.

4. Conclusion

This study found the values of scattering cross-sections and their variation in microwave frequencies lower than 10 GHz. The study calculated cross-sections of drops through passing microwave frequencies. Mie-scattering theory and Maxwell equations used to determine C_{ext} in a range of frequencies between 1 and 30 GHz. Maxwell's equations solved and simulated in COMSOL software (COMSOL Multiphysics Reference Manual, 1998) while scattering cross-sections simply calculated in MiePlot (MiePlot).

The results illustrated the difference between the variation of extinction cross-sections in higher and lower frequencies. The appearing of the peaks affects the attenuation-rainfall correlation when enough raindrops appear in the range of peak cross-sections. The change in the attenuation-rainfall relationship suggests a change in correlation coefficients in some particular frequencies and the validity of application of the rainfall-attenuation relationship in different frequencies. The suggestion is using varying coefficients for varying rainfall intensities and using a looped calculation to solve the A-R relationship.

Authors' agreement

We the undersigned declare that the manuscript entitled " Exploring the impact of rainfall intensity on the attenuation-rainfall relationship" is original, has not been fully or partly published before, and is not currently being considered for publication elsewhere.

We confirm that the manuscript has been read and approved by all named authors and that there are no other persons who satisfied the criteria for authorship but are not listed. We further confirm that the order of authors listed in the manuscript has been approved by the undersigned.

We understand that the Corresponding Author is the sole contact for the editorial process. The corresponding author " Saeid Esmaeil Nia" is responsible for communicating with the other authors about the process, submissions of revisions, and final approval of proofs.

CRediT authorship contribution statement

Saeid Esmaeil Nia: Writing – review & editing, Writing – original draft, Visualization, Validation, Software, Resources, Methodology, Investigation, Formal analysis, Conceptualization. **Ali Shokri:** Writing – review & editing, Supervision.

Declaration of competing interest

The authors declare that they have no known competing financial interests or personal relationships that could have appeared to influence the work reported in this paper.

Data availability

No data was used for the research described in the article.

References

[1] Saakian AS. Radio wave Propagation Fundamentals. Artech House; 2011.
[2] Louis J. Ippolito J. Radiowave Propagation in Satellite Communications. New York: Van Nostrand Reinhold Company Inc.; 1986.
[3] Whiton RC, Smith PL, Bigler SG, Wilk KE, Harbuck AC. History of Operational Use of Weather Radar by U.S. Weather Services. Part I: the Pre-Nexrad Era. American Meteorological Society; 1998. https://doi.org/10.1175/1520-0434(1998)013<0219:HOOUOW>2.0.CO;2. Jun.
[4] L.J. Ippolito, "NASA reference publication 1082(04) propagation effects handbook for satellite systems design satellite links with techniques for system design fourth edition," 1989.
[5] ITU-R, "P.837-6. Characteristics of precipitation for propagation modeling. Radiowave Propag 2012;6. vol[Online]. Available, https://www.itu.int/dms_pubrec/itu-r/rec/p/R-REC-P.837-7-201706-I!!PDF-E.pdf.
[6] Ryde JW, Ryde D. Attenuation of Centimetere and Millimetre Waves by Rain, Hail, Fogs, and Clouds. 2019. Rep. No. 8670," Wembley, England, 1945. Accessed: Jul. 03[Online]. Available, https://www.worldcat.org/title/attenuation-of-centimetre-and-millimetre-waves-by-rain-hail-fogs-and-clouds/oclc/897982788.
[7] Olsen RL, Rogers DV, Hodge DB. The aRb relation in the calculation of rain attenuation. IEEE Trans Antennas Propag 1978;26(2):318–29. https://doi.org/10.1109/TAP.1978.1141845.
[8] ITU-R, "Recommendation ITU-R P.838-3: specific attenuation model for rain use in prediction methods," 2005. [Online]. Available: https://www.itu.int/dms_pubrec/itu-r/rec/p/R-REC-P.838-3-200503-I!!PDF-E.pdf.
[9] Giuli D, Toccafondi A, Gentili GB, Freni A. Tomographic reconstruction of rainfall fields through microwave attenuation measurements. J Appl Meteorol 1991;30(9):1323–40. https://doi.org/10.1175/1520-0450(1991)030<1323:TRORFT>2.0.CO;2.
[10] Giuli D, Facheris L, Tanelli S. Microwave tomographic inversion technique based on stochastic approach for rainfall fields monitoring. IEEE Trans Geosci Remote Sens 1999;37(5):2536–55. https://doi.org/10.1109/36.789649.
[11] Holt AR, et al. Measurement of rainfall by dual-wavelength microwave attenuation. Electron Lett 2000;36(25):2099–101. https://doi.org/10.1049/el:20001468. Dec.

[12] Upton GJGJG, Holt ARR, Cummings RJJ, Rahimi ARR, Goddard JWFWF. Microwave links: the future for urban rainfall measurement? Atmos Res 2005;77 (1–4):300–12. https://doi.org/10.1016/J.ATMOSRES.2004.10.009. Sep.

[13] Messer H, Zinevich A, Alpert P. Environmental monitoring by wireless communication networks. Science (80-.) 2006;312(5774):713. https://doi.org/10.1126/science.1120034. May.

[14] Messer H. Rainfall monitoring using cellular networks. IEEE Signal Process Mag 2007;24(3). https://doi.org/10.1109/MSP.2007.361621.

[15] Leijnse H, Uijlenhoet R, Stricker JNM. Rainfall measurement using radio links from cellular communication networks. Water Resour Res 2007;43(3). https://doi.org/10.1029/2006WR005631. Mar.

[16] Huang H, Trömel S, Zhang P, Liu X, Pu K. Precipitation monitoring using commercial microwave links: current status, challenges and prospectives. Remote Sens 2023;15(19):4821. https://doi.org/10.3390/RS15194821. *VolPage*vol. 15, nop. 4821, Oct2023.

[17] Medeiros Filho FC, Cole RS, Sarma AD. Millimetre-wave rain induced attenuation: theory and experiment. IEE Proc H Microwaves, Antennas Propag 1986;133(4): 308–14. https://doi.org/10.1049/ip-h-2.1986.0054.

[18] Jiang H, Sano M, Sekine M. Weibull raindrop-size distribution and its application to rain attenuation. IEE Proc Microwaves, Antennas Propag 1997;144(3):197–200. https://doi.org/10.1049/ip-map:19971193.

[19] Atlas D, Ulbrich CW. Path- and area-integrated rainfall measurement by microwave attenuation in the 1–3 cm band. J Appl Meteorol 1977;16(12):1322–31. https://doi.org/10.1175/1520-0450(1977)016<1322:paairm>2.0.co;2. Dec.

[20] Oguchi T. Scattering from hydrometeors: a survey. Radio Sci 1981;16(5):691–730. https://doi.org/10.1029/RS016i005p00691. Sep.

[21] Best AC. The size distribution of raindrops. Q J R Meteorol Soc 1950;76(327): 16–36. https://doi.org/10.1002/qj.49707632704. Jan.

[22] Jameson AR, Kostinski AB. What is a Raindrop Size Distribution? American Meteorological Society; 2001. https://doi.org/10.1175/1520-0477(2001)082<1169:WIARSD>2.3.CO;2. Jun.

[23] Bringi VN, Chandrasekar V, Hubbert J, Gorgucci E, Randeu WL, Schoenhuber M. Raindrop Size Distribution in Different Climatic Regimes from Disdrometer and Dual-Polarized Radar Analysis. J Atmos Sci 2003;60(2):354–65. https://doi.org/10.1175/1520-0469(2003)060<0354:RSDIDC>2.0.CO;2. Jan.

[24] Sekhon RS, Srivastava RC. Doppler radar observations of drop-size distributions in a thunderstorm. J Atmos Sci 1971;28(6):983–94. https://doi.org/10.1175/1520-0469(1971)028<0983:droods>2.0.co;2. Sep.

[25] Jameson AR, Jameson AR. A comparison of microwave techniques for measuring rainfall. J Appl Meteorol 1991;30(1):32–54. https://doi.org/10.1175/1520-0450(1991)030<0032:ACOMTF>2.0.CO;2. Jan.

[26] R. Harikumar, "Rain drop size distribution (DSD): characteristics & developing an empirical model to derive DSD when rain rate alone is available chapter IV: DSD-Characteristics and empirical model," 2009. [Online]. Available: https://www.semanticscholar.org/paper/RAIN-DROP-SIZE-DISTRIBUTION-%28DSD%29%3A-CHARACTERISTICS-Harikumar/dbc587cb5a0cfb753dc5c87769263f19e612f2e8.

[27] Lam HY, Din J, Jong SL. Statistical and physical descriptions of raindrop size distributions in equatorial Malaysia from disdrometer observations. Adv Meteorol 2015;2015. https://doi.org/10.1155/2015/253730.

[28] Serio MA, Carollo FG, Ferro V. Raindrop size distribution and terminal velocity for rainfall erosivity studies. a review. J Hydrol 2019;576:210–28. https://doi.org/10.1016/j.jhydrol.2019.06.040. Sep. 01.

[29] Kotlarchyk M. Scattering theory. Encyclopedia of Spectroscopy and Spectrometry. Elsevier; 1999. p. 2074–84. https://doi.org/10.1006/rwsp.2000.0274.

[30] Leijnse H, Uijlenhoet R, Berne A, Leijnse H, Uijlenhoet R, Berne A. Errors and uncertainties in microwave link rainfall estimation explored using drop size measurements and high-resolution radar data. J Hydrometeorol 2010;11(6): 1330–44. https://doi.org/10.1175/2010JHM1243.1. Dec.

[31] Song K, Liu X, Gao T, He B. Raindrop size distribution retrieval using joint dual-frequency and dual-polarization microwave links. Adv Meteorol 2019;2019. https://doi.org/10.1155/2019/7251870.

[32] Berne A, Uijlenhoet R. Path-averaged rainfall estimation using microwave links: uncertainty due to spatial rainfall variability. Geophys Res Lett 2007;34(7): L07403. https://doi.org/10.1029/2007GL029409. Apr.

[33] Zinevich A, Messer H, Alpert P. Prediction of rainfall intensity measurement errors using commercial microwave communication links. Atmos Meas Tech 2010;3(5): 1385–402. https://doi.org/10.5194/amt-3-1385-2010. Oct.

[34] Rios Gaona MF, Overeem A, Leijnse H, Uijlenhoet R. Measurement and interpolation uncertainties in rainfall maps from cellular communication networks. Hydrol Earth Syst Sci 2015;19(8):3571–84. https://doi.org/10.5194/hess-19-3571-2015. Aug.

[35] Schleiss M, et al. The accuracy of weather radar in heavy rain: a comparative study for Denmark, the Netherlands, Finland and Sweden. Hydrol Earth Syst Sci. 2020;24 (6):3157–88. https://doi.org/10.5194/HESS-24-3157-2020. Jun.

[36] Doviak RJ…, Zrnić DS…. Doppler Radar and Weather Observations. Academic Press; 1984.Accessed: Sep. 10, 2024. [Online]. Available: http://www.sciencedirect.com:5070/book/9780122214202/doppler-radar-and-weather-observations.

[37] Sauvageot H. Rainfall measurement by radar: a review. Atmos Res 1994;35(1): 27–54. https://doi.org/10.1016/0169-8095(94)90071-X.

[38] Overeem A, Leijnse H, Uijlenhoet R. Rainfall monitoring using microwave links from cellular communication networks: the Dutch experience. 2018 IEEE Statl Signal Process Workshop (SSP) 2018:110–4. https://doi.org/10.1109/SSP.2018.8450708. Jun.

[39] van Leth TC, Leijnse H, Overeem A, Uijlenhoet R. Estimating raindrop size distributions using microwave link measurements. Atmos Meas Tech Discuss. 2019:1–27. https://doi.org/10.5194/amt-2019-51. no. AprilApr.

[40] Overeem A, Leijnse H, Uijlenhoet R. Two and a half years of country-wide rainfall maps using radio links from commercial cellular telecommunication networks. Water Resour Res 2016;52(10):8039–65. https://doi.org/10.1002/2016WR019412. Oct.

[41] Pudashine J, et al. Rainfall retrieval using commercial microwave links: effect of sampling strategy on retrieval accuracy. J Hydrol 2021;603:126909. https://doi.org/10.1016/j.jhydrol.2021.126909. Dec.

[42] Ishimaru A, Cheung RLT. Multiple-scattering effect on radiometric determination of rain attenuation at millimeter wavelengths. Radio Sci 1980;15(3):507–16. https://doi.org/10.1029/RS015i003p00507. May.

[43] Ishimaru A, Cheung RLT. Multiple scattering effects on wave propagation due to rain. Ann Des Telecommun 1980;35(11–12):373–9. https://doi.org/10.1007/BF03003515. Nov.

[44] Ishimaru A, Woo R, Armstrong JW, Blackman DC. Multiple scattering calculations of rain effects. Radio Sci 1982;17(6):1425–33. https://doi.org/10.1029/RS017i006p01425. Nov.

[45] Kesavan U, Islam MR, Abdullah K, Tharek AR. Rain attenuation prediction for higher frequencies in microwave communication using frequency scaling technique. In: 2014 International Conference on Computer and Communication Engineering; 2014. p. 217–9. https://doi.org/10.1109/ICCCE.2014.69. Sep.

[46] Lin SH. Statistical behavior of rain attenuation. Bell Syst Tech J 1973;52(4): 557–81. https://doi.org/10.1002/j.1538-7305.1973.tb01977.x.

[47] Ramos B, Cordero M, Hurtado K, Nunez A, D'Amico M. Rain rate estimation using a microwave link in Guayaquil City. In: 2017 IEEE 2nd Ecuador Technical Chapters Meeting; 2017. p. 1–6. https://doi.org/10.1109/ETCM.2017.8247522. *ETCM 2017*, Janvol. 2017-Janua.

[48] Ramos B, et al. Measuring rain with microwave links: a pilot experiment in Ecuador. In: 2015 IEEE-APS Topical Conference on Antennas and Propagation in Wireless Communications (APWC); 2015. p. 171–4. https://doi.org/10.1109/APWC.2015.7300149. Sep.

[49] Leijnse H, Uijlenhoet R, Stricker JNM. Microwave link rainfall estimation: effects of link length and frequency, temporal sampling, power resolution, and wet antenna attenuation. Adv Water Resour 2008;31(11):1481–93. https://doi.org/10.1016/j.advwatres.2008.03.004. Nov.

[50] Leijnse H, Uijlenhoet R, Berne A. Errors and uncertainties in microwave link rainfall estimation explored using drop size measurements and high-resolution radar data. J Hydrometeorol 2010;11(6):1330–44. https://doi.org/10.1175/2010JHM1243.1. Dec.

[51] C. and D. M. Office of the Minister of Broadcasting, "Allocation of radio spectrum for 5G mobile," 2019.

[52] C. and D. M. Office of the Minister of Broadcasting, "Early access to 5G radio spectrum," 2019.

[53] Serway RA, John W. Jewett J. Principles of Physics: A Calculus-Based Text. Thomson; 2005. https://doi.org/10.1017/CBO9781107415324.004.

[54] Waterman PC. Matrix formulation of electromagnetic scattering. Proc IEEE 1965; 53(8):805–12. https://doi.org/10.1109/PROC.1965.4058.

[55] Mishchenko MI, Travis LD, Mackowski DW. T-matrix computations of light scattering by nonspherical particles: a review. J Quant Spectrosc Radiat Transf 1996;55(5):535–75. https://doi.org/10.1016/0022-4073(96)00002-7. May.

[56] Mie G. Beiträge zur Optik Trüber Medien, Speziell Kolloidaler Metallösungen. Ann Phys 1908;330(3):377–445. https://doi.org/10.1002/andp.19083300302.

[57] Rayleigh Lord. "X. On the electromagnetic theory of light," London, Edinburgh. Dublin Philo. Mag. J Sci 1881;12(73):81–101. https://doi.org/10.1080/14786448108627074. Aug.

[58] Rayleigh Lord. " XXXIV. On the transmission of light through an atmosphere containing small particles in suspension, and on the origin of the blue of the sky ," London, Edinburgh. Dublin Philos. Mag J Sci 1899;47(287):375–84. https://doi.org/10.1080/14786449908621276. Apr.

[59] Barclay L. Propagation of Radiowaves. 2nd ed. London, United Kingdom: The institution of Engineering and Technology; 2003.

[60] Hecht E. Optics. 4th ed. Addison Wesley; 2002.

[61] Bohren CF, Huffman DR. Absorption and Scattering of Light by Small Particles. John Wiley & Sons, Inc.; 1983.

[62] Pruppacher HR, Beard KV. A wind tunnel investigation of the internal circulation and shape of water drops falling at terminal velocity in air. Q J R Meteorol Soc 1970;96(408):247–56. https://doi.org/10.1002/qj.49709640807. Apr.

[63] Beard KV. Terminal velocity adjustment for cloud and precipitation drops aloft. J Atmos Sci 1977;34(8):1293–8.Aug Accessed: May 01, 2019. [Online]. Available: http://journals.ametsoc.org/doi/abs/10.1175/1520-0469(1976)033<0851:TVASOC>2.0.CO;2.

[64] Beard KV. Terminal velocity and shape of cloud and precipitation drops aloft. J Atmos Sci 1976;33(5):851–64. https://doi.org/10.1175/1520-0469(1976)033<0851:TVASOC>2.0.CO;2. May.

[65] Marshall JS, Palmer WMK. The distribution of raindrops with size. J Meteorol 1948;5(4):165–6. https://doi.org/10.1175/1520-0469(1948)005<0165:TDORWS>2.0.CO;2. Aug.

[66] Gunn R, Kinzer GD. The terminal velocity of fall for water droplets in stagnant AIR. J Meteorol 1949;6(4):243–8. https://doi.org/10.1175/1520-0469(1949)006<0243:ttvoff>2.0.co;2. Aug.

[67] Strangeways I. Precipitation: Theory, Measurement and Distribution, 9780521851. Cambridge: Cambridge University Press; 2007. https://doi.org/10.1017/CBO9780511535772.

[68] J.E. McDonald, "The shape and aerodynamics of large raindrops," http://doi.org/10.1175/1520-0469(1954)011<0478:TSAAOL>2.0.CO;2, Dec. 1954.
[69] Jones DMA. The shape of raindrops. J Meteorol 1959;16(5):504–10. https://doi.org/10.1175/1520-0469(1959)016<0504:tsor>2.0.co;2. Oct.
[70] Platt CMR, Collins RL. LIDAR | Backscatter. Encyclopedia of Atmospheric Sciences. Elsevier; 2015. p. 270–6. https://doi.org/10.1016/B978-0-12-382225-3.00205-X.
[71] Seinfeld JH, Pandis SN, Noone K. Atmospheric chemistry and physics: from air pollution to climate change. Phys Today 1998;51(10):88–90. https://doi.org/10.1063/1.882420. Oct.
[72] Ishii S, et al. Rain attenuation in the microwave-to-terahertz waveband. Wirel Eng Technol 2016;7(2):59–66. https://doi.org/10.4236/WET.2016.72006. Apr.
[73] Ulbrich CW, Atlas D. Assessment of the contribution of differential polarization to improved rainfall measurements. Radio Sci 1984;19(1):49–57. https://doi.org/10.1029/RS019i001p00049. Jan.
[74] Oguchi T. Attenuation of electromagnetic wave due to rain with distorted raindrops. Part I. J Radio Res Lab Jap 1960;7(33):467–85.
[75] "MiePlot." (accessed Jan. 17, 2020).
[76] "COMSOL Multiphysics Reference Manual," 1998, Accessed: Jul. 09, 2021. [Online]. Available: www.comsol.com/blogs.
[77] Seybold John S. Introduction to RF Propagation. Hoboken, New Jersey: John Wiley & Sons, Inc.; 2005.
[78] O. Js, A. Ak, and A. At, "Dynamical model for deriving 1-min rain rate from various integrationtimes in a tropical region," 2016. [Online]. Available: https://api.semanticscholar.org/CorpusID:73554562.
[79] Omaki N, Kitao K, Imai T, Okumura Y. Investigation of Ray tracing accuracy in street cell environment in high-SHF band. In: 2014 International Symposium on Antennas and Propagation Conference Proceedings; 2014. p. 441–2. https://doi.org/10.1109/ISANP.2014.7026717.
[80] J.C. Lin and A. Ishimaru, "Propagation of millimeter waves in rain," 1971. Accessed: Mar. 18, 2020. [Online]. Available: https://apps.dtic.mil/docs/citations/AD0735291.
[81] Okamura S, Oguchi T. Electromagnetic wave propagation in rain and polarization effects. In: Proceedings of the Japan Academy Series B: Physical and Biological Sciences. 86; 2010. p. 539–62. https://doi.org/10.2183/pjab.86.539. Jun.
[82] Lin DP, Chen HY. Volume integral equation solution of extinction cross section by raindrops in the range 0.6-100 GHz. IEEE Trans Antennas Propag 2001;49(3):494–9. https://doi.org/10.1109/8.918626. Mar.
[83] Amarjit, Gangwar RPS. The finite element approach for evaluation of extinction cross-section of realistically distorted raindrops. Indian J Radio Sp Phys 2008;37:114–20.Accessed: Dec. 18, 2019. [Online]. Available: http://nopr.niscair.res.in/handle/123456789/2484.
[84] Liou KN. An Introduction to Atmospheric Radiation. Academic Press; 2002.
[85] Fu Q. Radiation transfer in the atmosphere | cloud-radiative processes. Encyclopedia of Atmospheric Sciences. Elsevier; 2015. p. 13–5. https://doi.org/10.1016/B978-0-12-382225-3.00338-8.
[86] Bohren CF, Huffman DR. Absorption and Scattering of Light by Small Particles. Wiley; 1998. https://doi.org/10.1002/9783527618156.
[87] Stamnes K, Thomas GE, Stamnes JJ. Radiative Transfer in the Atmosphere and Ocean. 2nd Editio. Cambridge University Press; 2017.Accessed: May 21, 2020. [Online] Available: https://books.google.co.nz/books?hl=en&lr=&id=DxR2nEp0CUIC&oi=fnd&pg=PR21&ots=SfMvaIl8B5&sig=OeeKciENe2mQQ2sVFhWvvAZDjGE&redir_esc=y#v=onepage&q&f=false.
[88] Seybold JS. Introduction to RF Propagation. 2005. https://doi.org/10.1002/0471743690. Hoboken, NJ, USA.
[89] García-Etxarri A, et al. Strong magnetic response of submicron Silicon particles in the infrared. Opt Express 2011;19(6):4815. https://doi.org/10.1364/oe.19.004815. Mar.
[90] H. Laurell and J. Hillborg, "Towards a nanometer thick flat lens," 2018.
[91] Sekine M, Lind G. Rain attenuation of centimeter, millimeter and submillimeter radio waves. In: 12th European Microwave Conference; 1982. p. 584–9. https://doi.org/10.1109/EUMA.1982.333124. *1982*, Oct.